

A quantitative model based on an experimental study for the magnetoelectric coupling at the interface of cobalt ferrite–barium titanate nanocomposites

M. Rasly^{1,3} · M. Affi² · A. E. Shalan³ · M. M. Rashad³

Received: 15 August 2016 / Accepted: 3 April 2017 / Published online: 10 April 2017
© Springer-Verlag Berlin Heidelberg 2017

1 Introduction

Multiferroic (MF) composites, which possess simultaneously ferromagnetic and ferroelectric ordering, have recently stimulated much technological interest by their potential applications in the areas of memory devices, magnetic field sensors, transducers, phase shifters, current sensors, filters, resonators, etc. Generally, coupling interaction between these two phases engenders the material new functions most likely the magnetoelectric (ME) effect [1–4]. This effect is a product property of the constituent phases and is extrinsic in nature as none of the phases exhibit this effect individually [5]. Subsequently, in these composites, the coupling between two phases is mediated by strain; on application of the magnetic field, the magnetic phase undergoes change in shape and the resulting strain is passed to the ferroelectric phase, producing stress which in turn generates induced voltage due to the piezoelectric effect [6].

Plainly, good mechanical coupling between the ferrite and ferroelectric grains in the composites is required to

achieve a high ME signal. The mechanical coupling between grains in ME composites could be increased by increasing the sintering temperature [7]. However, the highly sintering temperature would produce another problem. It is known that increasing the annealing temperature leads to increase amount of Fe²⁺ ions in ferrite ceramics. Therefore, it decreases the electric resistivity and so affecting negatively to achieve a high ME response [8]. Therefore, different combinations of MF composites have been previously studied; they proved that materials in its nature should exhibit high magnetostriction and piezoelectric coefficients to generate high ME output [3, 4]. Meanwhile, the resistivity of the constituent phases is also a key factor and prerequisite to achieve a high ME response as discussed [9].

Consequently, based on the previous published literature; the highly ferroelectric barium titanate BaTiO₃ (BTO) is more suitable for such application because of its high dielectric permittivity and resistivity of the order of ($\sim 10^9$ Ωcm) [10, 11]. Besides, it also offers the advantage of being nontoxic and hence it is environment friendly. We recently investigated the dependence of optical and dielectric properties of barium strontium titanate nanopowders [12] along with the influence of incorporating transition metal ion on its dielectric and magnetic properties [13]. Apart from that, the spinel cobalt ferrite CoFe₂O₄ (CFO) is advisable as the magnetic constituent due to it has a high magnetostriction force [14] and moderate ferromagnetic properties among other ferrites [15]. Therefore, a great deal of effort has been directed to study the ME coupling properties into CFO–BTO nanocomposites. However, searching on literature, all of these studies based on the qualitative analysis of the ME properties at interface.

Electronic supplementary material The online version of this article (doi:10.1007/s00339-017-0954-x) contains supplementary material, which is available to authorized users.

✉ M. Rasly
m.rasly85@gmail.com

¹ Graduate School of Information Science and Technology, Hokkaido University, Sapporo 060-0814, Japan

² Ultrasonic Laboratory, National Institute for Standards, Tersa Street, P.O. Box 136, El-Giza 12211, Egypt

³ Central Metallurgical Research and Development Institute (CMRDI), P.O. Box: 87, Helwan 11421, Egypt

The purpose of this study is twofold. The first is to experimentally investigate the compositional dependence on structural, microstructure, magnetic and magnetoelectric coupling properties of $[(1-x) \text{CFO} + (x) \text{BTO}]$: $x = 0.0, 0.25, 0.50, 0.75$ and 1] nanocomposites at room temperature (RT). The second purpose is to quantitatively model the ME coupling at interface between CFO and BTO based the argument analysis, leads to a fuller understanding for the ME coupling on these CFO–BTO nanocomposites. This paper is organized as follows. Section 2 describes our experimental methods. In Sect. 3.1, we investigate the structural and the microstructural properties of $[(1-x) \text{CFO} + (x) \text{BTO}]$: $x = 0.0, 0.25, 0.50, 0.75$ and 1] nanocomposites. In Sect. 3.2, we study the magnetic properties and ME coupling between CFO and BTO nanocomposites. In Sect. 3.3, we would propose a quantitative model for the ME coupling at the interface between CFO and BTO phases within the nanocomposites. This gives us an important insight towards an understanding of the origin of the ME switching properties, especially, interfacial coupling, and the conditions needed to tailor the nanocomposites for the ME switching applications.

2 Experimental

2.1 Materials and procedure

CoFe_2O_4 nanopowders were prepared at room temperature using simple co-precipitation (CP) method. Stoichiometric ratios of anhydrous ferric chloride (FeCl_3) and cobalt chloride (CoCl_2) were dissolved in deionized water at Fe:Co molar ratio 2:1. The ferrite precursor was precipitated from this mixture by adding 5 M sodium hydroxide solution (NaOH) to pH 11. The aqueous suspension was stirred gently for 15 min to achieve a good homogeneity and to attain a stable pH condition. A (brownish) co-precipitate was obtained thereafter; it was boiled on hot plate magnetic stirrer for 1 h till obtaining black-colored CoFe_2O_4 precursor. The precursor was filtered off, washed with deionized water and dried in open air overnight.

BaTiO_3 (BTO) powders were prepared using sol gel auto-combustion (SGA) method. Stoichiometric ratios of barium nitrate $\text{Ba}(\text{NO}_3)_2$ and titanium isoperoxide were dissolved in aqueous solution and then stirred for 15 min on hot plate magnetic stirrer. An appropriate amount of citric acid solution was added gradually into the solution at 70°C to achieve a good homogeneity of metal ions. Then, ammonia solution was dropped gently into the solution to adjust the pH value to 7. The formed solution was evaporated at 70°C with constant stirring to form a viscous resin. Then, the transparent homogeneous sol was dried at 100°C for 6 h, resulting in a dried gel-citrate precursor.

After that, the precursor was thermally annealed at 900°C for 2 h.

Particulate magnetoelectric composites having the general formula $[(1-x) \text{CFO} + (x) \text{BTO}]$: $x = 0.0, 0.25, 0.50, 0.75$ and 1.0], have been prepared using a ball milling technique; high-speed laboratory ball mill (PM100, Retsch GmbH, Haan, Germany). The ball-to-powder ratio was about 10:1. For each composition “ x -percentage” was pre-weighed then introduced to the ball such that the total weight for each composite was fixed to be 1 g. Mixed powder was taken out from the mill after 15 min, then introduced into a tool steel die for hydraulic pressing (3 Ton) using a ABCO MEGA hydraulic Press. The thickness and diameter of the output pellets were 1.5 and 10 mm, respectively. To avoid damaging during physical characterization, those pellets were annealed at 250°C for half an hour, polished and finally coated with a silver paste.

2.1.1 Physical characterization

The phases of the prepared powders were identified from the XRD patterns collected at room temperature (RT) using a Bruker axis D8 diffractometer with Cu K_α ($\lambda = 1.5406 \text{ \AA}$) radiation in 2θ range from 20 to 80° . The particle morphology was investigated by field emission scanning electron microscope (FE-SEM, FEI Company, Quanta FEG 250). The magnetic properties of the nanocomposites were carried out at room temperature using a vibrating sample magnetometer (VSM, Lake Shore 7410, USA). Handmade circuit was used to investigate the electric polarization along with the magnetoelectric coupling property between two phases [16]. Such that the magnetoelectric coefficient ($\alpha_E = \frac{dE}{dH}$) was characterized by the induced electric field E under an applied magnetic field H (consists of alternating magnetic field H_{ac} ($f = 10 \text{ kHz}$) and DC bias magnetic field (H_{dc} 5 Oe), which causes the magnetoresistive material to stress the piezoelectric material. The pellets were oriented along the in-plane direction with respect to the ac magnetic field and the magnetic bias. The induced electric field E was detected using a lock-in amplifier (Signal Recovery, 5210 Lock-In Amplifier).

3 Results and discussion

3.1 Structural analysis

3.1.1 X-ray analysis and material porosity

Figure 1 depicts the XRD patterns of the prepared nanocomposites, consisting of a spinel co-ferrite (CoFe_2O_4 –CFO) mixing with a perovskite Ba-titanate (BaTiO_3 –BTO) for different weight percentages; $[(1-x)$

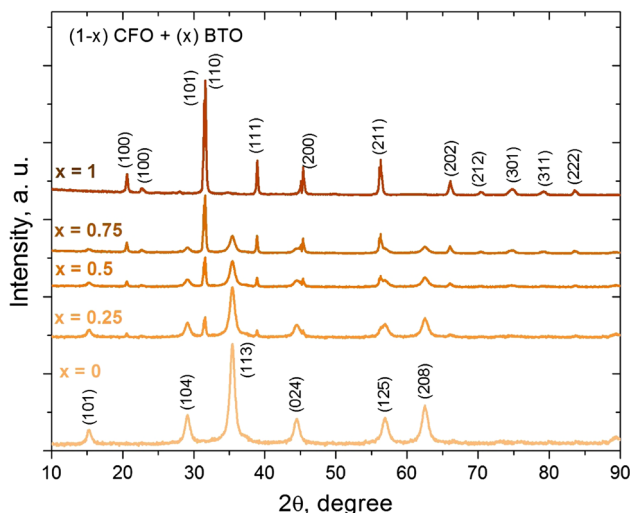


Fig. 1 XRD patterns of the produced [(1-x) CoFe₂O₄ (CFO) + (x) BaTiO₃ (BTO): x = 0.0, 0.25, 0.50, 0.75, and 1.0) nanocomposites

CFO + (x) BTO: x = 0.0, 0.25, 0.5, 0.75, and 1]. For x = 0.0 and 1, patterns show single crystalline CFO and BTO phases; all diffraction peaks are fully indexed with their reference cards (JCPDS# 79-1744) and (JCPDS# 79-2265), respectively. The relative intensities for each constituent phase increases (decreases) as its content increases (decreases) in the composites. For instance, the relative intensities of main peaks [(104), (113), (024), (125) and (208)] referring to CFO phase decrease gradually as the weight percentages x increase from x = 0 to x = 1. Alternatively, the relative intensities of main peaks [(101), (110), (111), (200), (200) and (211)] corresponding to BTO phase increase until reaching pure BTO at x = 1. No unidentified peaks are observed, suggesting that no chemical reactions have occurred either due to milling or post-annealing at 250 °C. The unit cell of the CFO phase is well-described with the cubic structure belonging to the space group *Fd3m*, whereas the BTO phase shows the tetragonal structure with space group *P4mm*. The structural parameters are given in Sect. 1 in the supplementary information, (SI). The lattice parameters of CFO and BTO are a = 8.33 Å, and a = 3.39 Å and c = 4.00 Å (c/a = 1.17), respectively. Moreover, the lattice parameters of the nanocomposites (Table S1, SI) are almost equal to those of the constituent phases, confirming that no structural changes have occurred.

The theoretical density of the prepared nanocomposites was calculated using the rule of mixture as following [17]:

$$\rho_{th} = \rho_{CFO}V_{CFO} + \rho_{BTO}V_{BTO}, \tag{1}$$

where V_{CFO} and V_{BTO} are the volume fractions of CoFe₂O₄ and BaTiO₃, respectively. Since the total mass for each composite was fixed to be 1 g, then the volume fraction of

Table 1 Theoretical and apparent densities of [(1 - x) CoFe₂O₄ (CFO) + (x) BaTiO₃ (BTO): x = 0.25, 0.50 and 0.75, respectively] nanocomposites along with their porosity percentage

Weight ratios, x	Theoretical density, ρ_{th} (g/cm ³)	App. density, ρ_{ex} (g/cm ³)	Porosity, P (%)
0	5.41	4.68	13.49
0.25	6.61	5.315	19.59
0.50	6.91	5.95	13.89
0.75	7.65	6.58	13.99
1	8.40	7.21	14.17

each phase at nanoscale could be expressed by its weight percentage x.

The experimental density (ρ_{ex}) was measured using Archimedes principle as in following expression:

$$\rho_{ex} = \frac{W_{air}}{W_{air} - W_{liq}} \times \rho_{liq}, \tag{2}$$

where W_{air} and W_{liq} are the weight of samples in air and liquid medium (ethanol), respectively. The density (ρ_{liq}) of ethanol is (0.79 g/cc). Porosity percentage (P, %) was calculated using the relation:

$$P(\%) = \left[1 - \frac{\rho_{ex}}{\rho_{th}} \right] \times 100. \tag{3}$$

The calculated values are listed in Table 1. Higher porosity percentage, % of BTO than CFO phase is reasonable and it might be attributed to usage of the auto-combustion method and its mechanism, producing more porous phase in comparison to precipitation technique [18]. Correspondingly, the porosity percentage, % of intermediate-phases increases as BTO content increases.

3.1.2 Microstructures

FE-SEM pictures of (a) pure CoFe₂O₄ (x = 0.0), (b) intermediate nanocomposite sample (x = 0.5) and (c) pure BaTiO₃ (x = 1) are shown in Fig. 2 together with their corresponding size distributions. The cubical-like structure was observed for all three samples. Giving more insight, one can observe that the size of particle increases as weight percentage x increases, whereas densification of particle decreases. It can be directly explained due to increasing the content of BTO comparative to CFO phase within the whole composite as x increases. Based on the analysis of the particle size distributions, the mean diameter increased from “~20 nm” at x = 0.0 to “~30 nm” at x = 0.25 and finally “~40 nm” at x = 1. A relatively high annealing temperature (900 °C) along with the long annealing time (2 h) is required to crystallize the single-phase perovskite BaTiO₃ is the reason why the particle size enlargement. This also led to decrease in

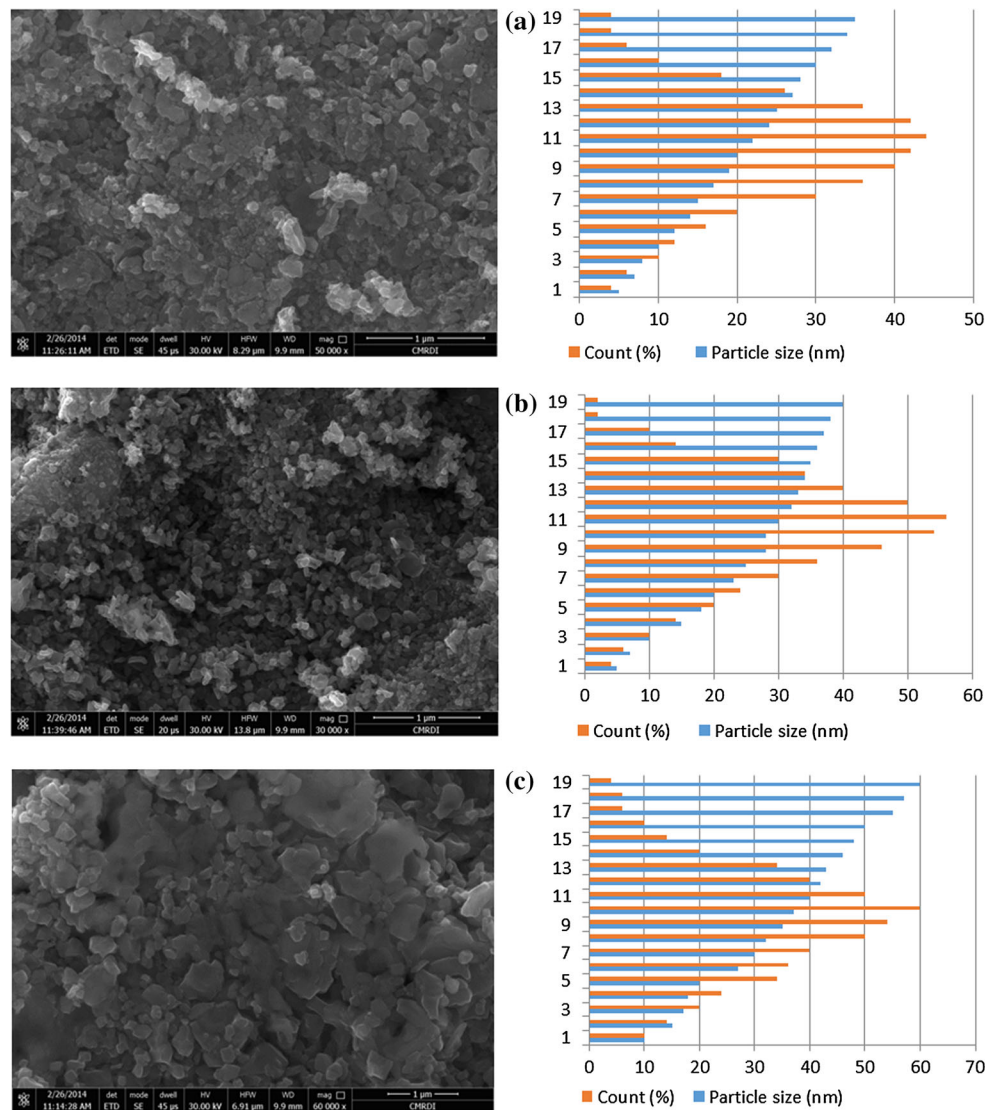


Fig. 2 FE-SEM micrographs of synthesized nanoparticles with corresponding size distributions: **a** pure CoFe₂O₄, $x = 0.0$; **b** intermediate sample, $x = 0.5$ and **c** pure BaTiO₃, $x = 1$

the density of particles per unit volume as the particle size increased with increasing x percentage. Last but not least, this result is also consistent with the X-ray diffraction results, showing that the crystallite size is also increasing with increasing x percentage.

3.2 Magnetic and magnetoelectric properties

3.2.1 Magnetic properties

From the measurement of M - H hysteresis loops (Fig. S1) at RT and related magnetic parameters (Table S2) given in Sect. 2 (SI), we directly plot the magnetization M (emu/g) and the coercivity H_c (Oe) dependence on the x -content for different nanocomposites; [(1 - x) CFO + (x) BTO: $x = 0.0, 0.25, 0.5$ and 0.75], as shown in Fig. 3. The soft

ferromagnetic property of the CFO content was decreased as increasing the BTO content within the whole matrix, the net magnetization gradually decreased as x increased. Remarkably, those two phases would produce antiferromagnetic coupling that causes a decrease in the net magnetization. Aside from that, this coupling could hinder the magnetization reversal process because of difficulty for the domain wall rotation. Therefore, a highly magnetostatic energy ($U = -\mathbf{M} \cdot \mathbf{H}$) is required to reset zero magnetization, leading to that M decreased and H_c increased as increasing x -content [19, 20]. Moreover, it is stated that ME composites that homogeneously dispersed lower fraction of magnetic component of CFO with respect to higher percentage of porosity BTO lead to the interrupted magnetic interaction between ferrite grains, resulting in the increase of coercivity [21].

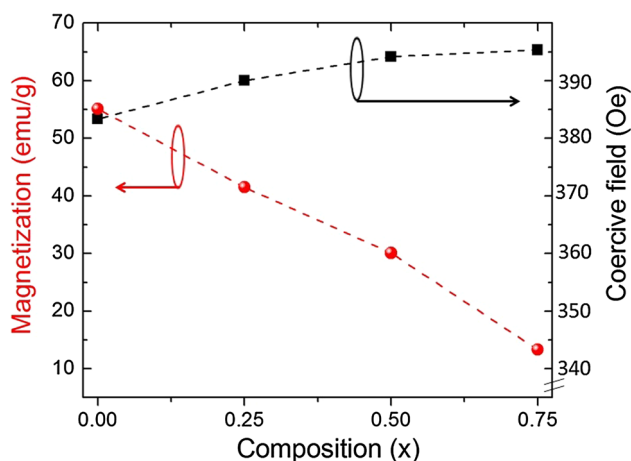


Fig. 3 The dependence of the magnetization M and the coercivity H_c on x -content for different nanocomposites $[(1-x)\text{CFO} + (x)\text{BTO}]$: $x = 0.0, 0.25, 0.50$ and 0.75] measured at room temperature

3.2.2 Magnetoelectric properties

Herein, based on P - E hysteresis loops (Fig. S2) measured at RT and related electric parameters (Table S3) as shown in Sect. 3 (SI), the dependence of the electric polarization P ($\mu\text{C}/\text{cm}^2$) and the coercive field E_c (KV/cm) on the x -content for different nanocomposites; $[(1-x)\text{CFO} + (x)\text{BTO}]$: $x = 0.0, 0.25, 0.5, 0.75$, and 1 , is given in Fig. 4. The polarization maxima was smaller for the nanocomposite sample with large content of CFO; the maximum value was $18.1\ \mu\text{C}/\text{cm}^2$ for pure BTO sample whereas the lowest value was $0.5\ \mu\text{C}/\text{cm}^2$ for $x = 0.0$. Definitely, this was due to the gradual degradation of the ferroelectric BTO phase with increasing CFO content inside the overall matrix. The free movement of the electric dipole moments with the applied electric field was also hindered owing to the strengthen of the domain wall

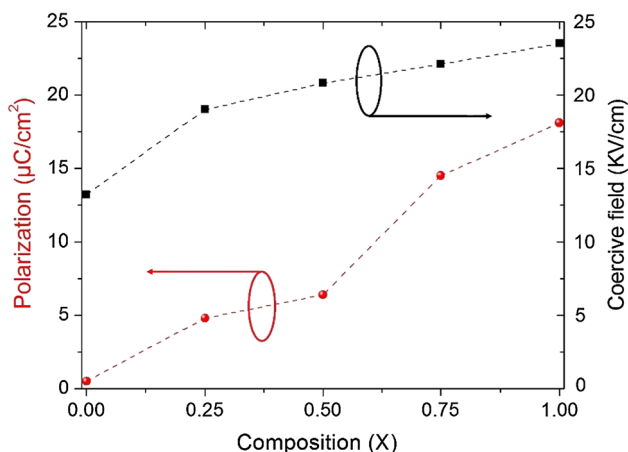


Fig. 4 The dependence of the polarization P and the coercivity H_c on x -content for different nanocomposites $[(1-x)\text{CFO} + (x)\text{BTO}]$: $x = 0.0, 0.25, 0.50, 0.75$ and 1] measured at room temperature

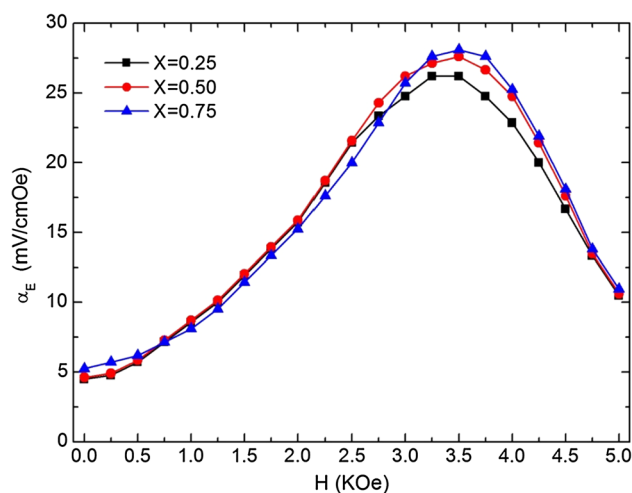


Fig. 5 Dependence of the magnetoelectric coefficient α_E on the H_{bias} of the $[(1-x)\text{CoFe}_2\text{O}_4\text{(CFO)} + (x)\text{BaTiO}_3\text{(BTO)}]$: $x = 0.25, 0.50$ and 0.75 nanocomposites at an AC magnetic frequency $10\ \text{kHz}$

rotation with increasing the porosity percentage of BTO in a similar situation to that the magnetic field controls magnetic properties. As a consequence, the electric coercivity E_c increased as BTO increased.

In the following discussion, we will identify and focus on the coupling properties between CFO and BTO phases. The dependence of ME coefficient α_E of $[(1-x)\text{CFO} + (x)\text{BTO}]$: $x = 0.25, 0.50$ and 0.75] nanocomposites as a function of H_{bias} at an ac magnetic frequency with $10\ \text{kHz}$ is presented in Fig. 5. As a normal behavior of the α_E , for all investigated samples, α_E has initially a small value ($\sim 5\ \text{mV}/\text{cm Oe}$) near the zero magnetic bias. Then, with the increase in H_{bias} , α_E was increased linearly and reached to its maximum value approximately at $H_{\text{bias}} = 3.5\ \text{kOe}$. The ME coefficients observed at the maxima for $x = 0.25, 0.50$ and 0.75 composites are $5.7, 25.85, 26.90$ and $28.55\ \text{mV}/\text{cm Oe}$, respectively, these values are relatively larger than that reported in Ref [22, 23]. Thereafter, α_E decreased as H_{bias} increased.

3.2.3 The quantitative modeling

In this section, we would turn to propose a quantitative model to explain the dramatic behavior of ME coupling based on three case-studies: case 1, 2 and 3, corresponding to sample of $x = 0.25, 0.50$ and 0.75 , respectively. For each case study α_E increased with increasing BTO content and shifted a little bit to the high H_{bias} until the normal decaying mechanism. This is might be attributed to the increase in the ME interaction between CFO and BTO nanoparticles than the mutual magnetic exchange interaction between CFO nanoparticles inside the matrix. In fact, the particle size of CFO is smaller than that of BTO, leading to larger surface area of CFO than that of BTO

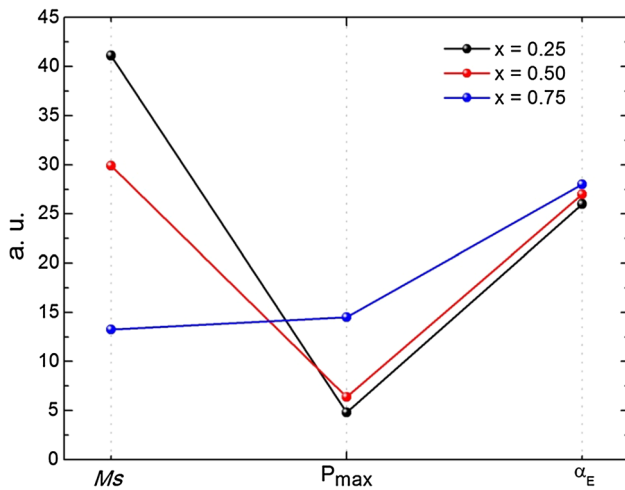


Fig. 6 Function argument on saturation magnetization (M_s), maximum polarization (P_s) and ME coefficient (α_E)

[24]. Correspondingly, the number of magnetic dipole moments distributed over the surface of CFO nanoparticles increased as x increased. Furthermore, the porosity percentage, % of nanocomposites was increased with BTO content. Thus, the direct–direct interaction between magnetic CFO nanoparticles inside matrix increased and it has much more possibility to occur rather than the indirect “ME interaction” with the other BTO nanoparticles, i.e., there is a certain limit for CFO content to maximize ME coupling mechanism.

A function argument on M_s , P_{max} and α_E is constructed for the intermediate samples of $x = 0.25, 0.50$ and 0.75 and results as shown in Fig. 6. It is clear that, for the nanocomposite of $x = 0.75$, both M_s and P_{max} are relatively in a balance state compared to that of $x = 0.50$ and $x = 0.25$. Again, as it proposed in Section A, at an ultimate-scale of integration: the particle size is approximately equal to its volume. It can be given also from the particle size distribution that the average particle size of BTO nanoparticles is ($\theta_1 \sim 40$ nm) and that of CFO nanoparticles is ($\theta_2 \sim 20$ nm) approximately.

Herein, let us consider that each composite has a matrix of a cubic volume ($V = 1000 \text{ nm}^3$). In addition, the volume fraction of CFO and BTO nanoparticles inside matrix volume are given by δ_1 and δ_2 , respectively. Consequently,

the number of BTO nanoparticles inside the matrix can be expressed by

$$N_1 = \text{CFO No} = \frac{\delta_1 V}{\theta_1}, \tag{4}$$

and the number of CFO nanoparticles inside matrix is given by

$$N_2 = \text{BTO NO} = \frac{\delta_2 V}{\theta_2}. \tag{5}$$

Then, the total number of nanoparticles inside each matrix is

$$N_t = N_1 + N_2 \tag{6}$$

while the difference is

$$N_d = |N_1 - N_2|. \tag{7}$$

Furthermore, the difference percentage between two constituents is expressed by

$$\text{DP, \%} = \frac{N_d}{N_t} \times 100, \%. \tag{8}$$

Calculated data are listed in Table 2 and its description is shown in Fig. 7. Results showed that DP, % is inversely proportional to x , i.e., the possibility of interaction between dissimilar nanoparticles (BTO/CFO) increases as x increases. This means that, at $x = 0.75$, all CFO nanoparticles are well distributed and filled the interstitial sites between BTO nanoparticles inside the matrix.

Basically, for the ME composites under off-resonance conditions, the change in α_E is given by the following expression [23, 24]:

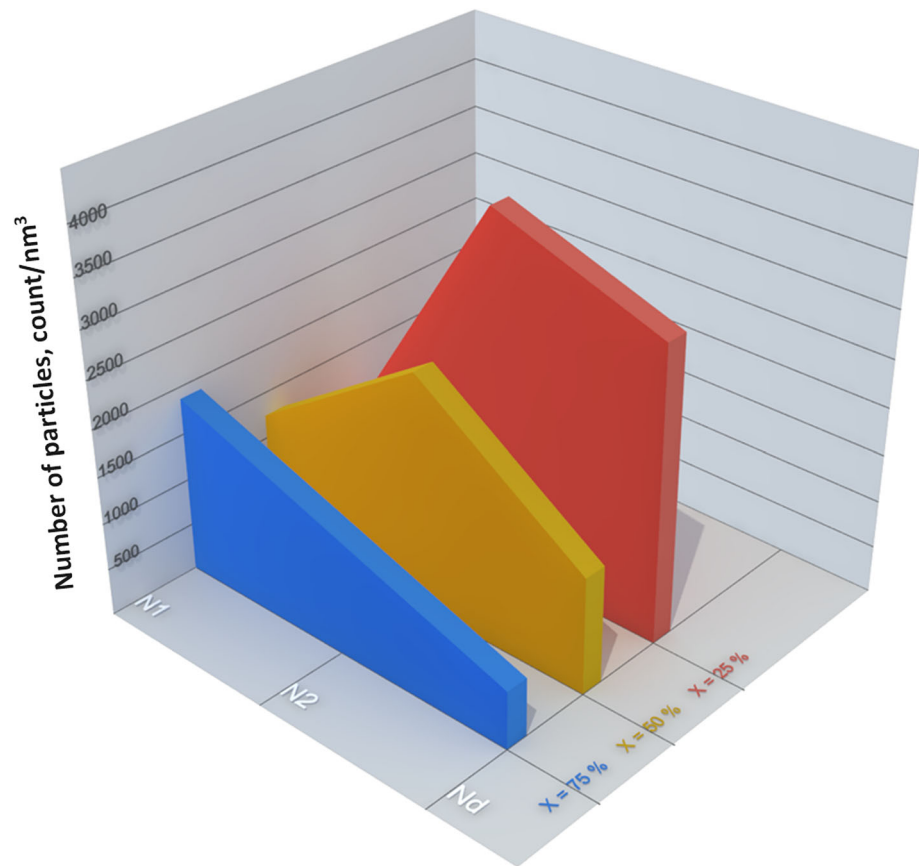
$$\alpha_E = \delta_1 \left(\frac{ds}{dH} \right)_{\text{CFO}} \delta_2 \left(\frac{dE}{ds} \right)_{\text{BTO}}, \tag{9}$$

where $\frac{ds}{dH}$ is the change in strain with magnetic field, and $\frac{dE}{ds}$ is the resulting electric field. This means that the ME effect is a product property between magnetostrictive (resulting from CFO content) and piezoelectric (resulting due to BTO content) energies, i.e., the maximum α_E depends on the relative volume fractions of two constituents. Accordingly, the optimum CFO volume fraction required to give rise to the highest $\alpha_E = 28 \text{ mV/cm Oe}$ is at $x = 0.75$. Thereafter, with a further increase in CFO content, although the

Table 2 Calculated numbers of CFO, BTO nanoparticles, along with total and difference percentage for the intermediate [(1 - x) CoFe₂O₄ (CFO) + (x) BaTiO₃ (BTO): $x = 0.25, 0.50$ and 0.75 , respectively] nanocomposites

Volume fraction, nm ³		Number of particles		Total number of particles, N_t	Difference number, N_d	Difference percentage, DP, %
δ_1	δ_2	N_1	N_2			
0.75	0.25	1875	1250	3125	625	20
0.50	0.50	1250	2500	3750	1250	33
0.25	0.75	625	3750	4375	3125	72

Fig. 7 The difference in the particle numbers N_d as a function of x -content for the intermediate $[(1-x)\text{CoFe}_2\text{O}_4(\text{CFO}) + (x)\text{BaTiO}_3(\text{BTO})]$: $x = 0.25, 0.50$ and 0.75 , respectively] nanocomposites



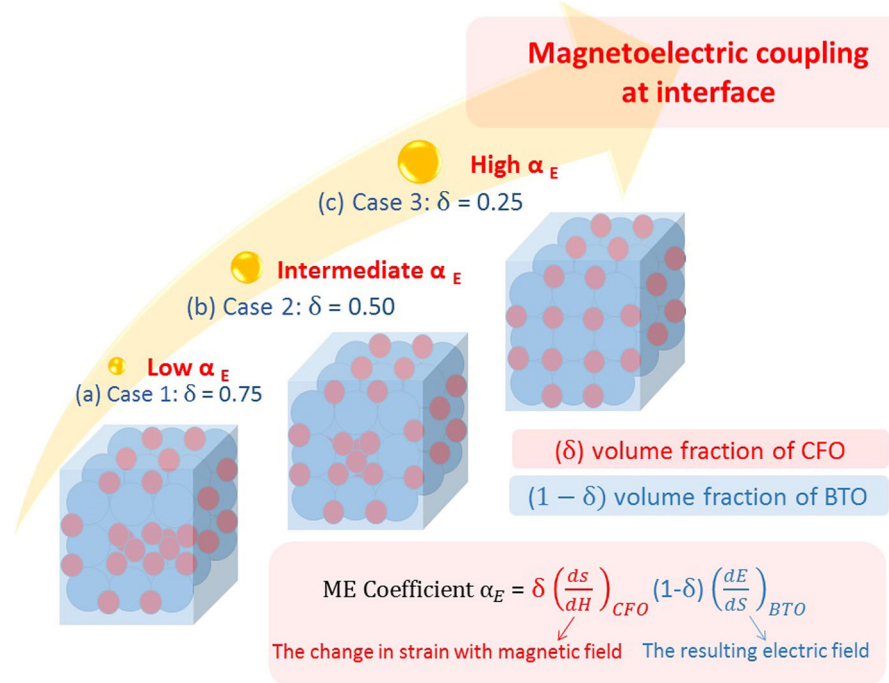
induced strain tends to increase, the high concentration of the low-resistance ferrite phase makes the samples difficult to be polarized. This causes a low piezoelectricity and causes the charges developed in the BTO phase to leak through this low-resistance phase path, resulting in a reduction of α_E at $x = 0.50$ and finally reached the lowest value at $x = 0.25$. In this regime, the spin-polarized charge density formed at the surface of CFO in the vicinity of the BTO interface acts as a torque on the magnetic moments of the CFO constituents, leading to that the direct-direct interaction at CFO-BTO interface gradually increases from $x = 0.25 \Rightarrow 0.5 \Rightarrow 0.75$. For each composite, the ME coupling of ferromagnetic and piezoelectric phases has degrees of freedom produced as a result of the influence of the mother piezoelectric matrix on the exchange coupling constant via screening of the intragrain and intergrain Coulomb interactions. As a consequence, a possible mechanism for ME coupling of CFO-BTO interface might be influenced by the screening effect [25]. The spin-polarized charge density formed in the CFO in the vicinity of the CFO/BTO interface acts with a torque on the magnetic moments in the CFO, resulting in an electric polarization that couples the CFO to the BTO for the whole matrix. This effect is supported by increasing material porosity. The polarizability is preferable around lattice defects (voids and

imperfections) and porosity regions. Since, porosity percentage increased as x -content increased, the resulting electric field, arising from this polarization, actually stems from the BTO surface, which acts as a provider for producing spin spiral with CFO, i.e., the ME coupling at the BTO/CFO interface is inversely proportional to the screening effect. In other words, the number CFO nanoparticles that can directly interact with BTO nanoparticles inside the matrix increased as x increased. On the contrary, its possibility to interact with similar CFO nanoparticles increased as x decreased as illustrated in Fig. 8 (case 1, 2 and 3, respectively). All in all, this function argument could reproduce the physical explanation of the proposed model based on Eqs. 4–9, giving rise to a quantitative analysis for prior studies on the magnetoelectric switching studies and the interplay of the ferroelectricity [1, 22–25]. Moreover, these findings enable the control of the inter-conversion of energies stored in electric and magnetic fields for future magnetoelectric switching applications.

4 Conclusions

The results can be summarized as follows:

Fig. 8 Schematic description of the magnetoelectric coupling at the interface of $[(1-x)\text{CoFe}_2\text{O}_4\text{ (CFO)} + (x)\text{BaTiO}_3\text{ (BTO)}]$ nanocomposites, where **a** case 1: $x = 0.25$; **b** case 2: $x = 0.5$ and **c** case 3: $x = 0.75$, respectively



1. Multiferroic nanocomposites of $[(1-x)\text{CoFe}_2\text{O}_4\text{ (CFO)} + (x)\text{BaTiO}_3\text{ (BTO)}]$: $x = 0.0, 0.25, 0.50, 0.75$ and 1] have been successfully synthesized.
2. The cubical-like structure was observed for CFO–BTO nanocomposites. Moreover, it was observed that the porosity percentage, % was increased as x -content increased.
3. As increasing volume ratio of BTO content relative to CFO content, net magnetization decreased whereas maximum polarization increased. Moreover, a type of antiferromagnetic coupling is magnetically raised up, leading to hinder the magnetization reversal process and hence coercivity increased.
4. A quantitative model for the ME coupling at the interface of CFO–BTO is established and its analysis is reproduced using a functional argument based on magnetization, polarization and ME coefficient. Results showed that the reason why a maximum ME coefficient α_E at $x = 0.75$ is the direct–direct interaction occurring in the vicinity of CFO/BTO, which is inversely proportional to the screening effect.
5. These findings present full-understanding for controlling the inter-conversion of energies stored in electric and magnetic fields for several electronic applications as magnetic field sensors and transducers.

References

1. K.C. Verma, S.K. Tripathi, R.K. Kotnal, Magneto-electric/dielectric and fluorescence effects in multiferroic $x\text{BaTiO}_3$ – $(1-x)\text{ZnFe}_2\text{O}_4$ nanostructures. *RSC Adv.* **4**, 60234–60242 (2014)
2. H. Trivedi, V.V. Shvartsman, D.C. Lupascu, M.S.A. Medeiros, R.C. Pullar, A.L. Kholkin, P. Zelenovskiy, A. Sosnovskikh, V.Y. Shur, Local manifestations of a static magnetoelectric effect in nanostructured BaTiO_3 – $\text{BaFe}_{12}\text{O}_{19}$ composite multiferroics. *Nanoscale* **7**, 4489–4496 (2015)
3. L.-J. Zhai, H.-Y. Wang, Effects of magnetic correlation on the electric properties in multiferroic materials. *J. Magn. Magn. Mater.* **377**, 121–125 (2015)
4. R. Tadi, Y.-I. Kim, D. Sarkar, C. Kim, K.-S. Ryu, Magnetic and electrical properties of bulk $\text{BaTiO}_3 + \text{MgFe}_2\text{O}_4$ composite. *J. Magn. Magn. Mater.* **323**(5), 564–568 (2011)
5. R. Grigalaitis, M.M.V. Petrović, J.D. Bobić, A. Dzunuzovic, R. Sobiestianskas, A. Brilingas, B.D. Stojanović, J. Banys, Dielectric and magnetic properties of BaTiO_3 – NiFe_2O_4 multiferroic composites. *Ceram. Int.* **40**, 6165–6170 (2014)
6. G. Srinivasan, T. Rasmussen, R. Hayes, Magnetoelectric effects in ferrite-lead zirconate titanate layered composites: the influence of zinc substitution in ferrites. *Phys. Rev. B* **67**, 014418 (2003)
7. J. Ryu, A. Vazquez Carazo, K. Uchino, H. Kim, Piezoelectric and magnetoelectric properties of lead zirconate titanate/Ni-ferrite particulate composites. *J. Electroceramics* **7**, 17–24 (2001)
8. B.K. Bammannavar, L.R. Naika, R.B. Pujar, B.K. Chougule, Resistivity dependent magnetoelectric characterization of $\text{Ni}_{0.2}\text{Co}_{0.8}\text{Fe}_2\text{O}_4 + \text{Ba}_{0.8}\text{Pb}_{0.2}\text{Zr}_{0.8}\text{Ti}_{0.2}\text{O}_3$ composites. *J. Alloys Compd.* **477**, L4–L7 (2009)
9. J.V.D. Boomgaard, R.A.J. Born, A sintered magnetoelectric composite material BaTiO_3 – $\text{Ni}(\text{Co}, \text{Mn})\text{Fe}_2\text{O}_4$. *J. Mater. Sci.* **13**, 1538–1548 (1978)
10. M.T. Buscaglia, V. Buscaglia, M. Viviani, J. Petzelt, M. Savinov, L. Mitoseriu, A. Testino, P. Nanni, C. Harnagea, Z. Zhao, M. Nygren, Ferroelectric properties of dense nanocrystalline BaTiO_3 ceramics. *Nanotechnology* **15**, 1113–1117 (2004)
11. D. Sallagoity, C. Elissalde, J. Majimel, R. Berthelot, U.C. Chung, N. Penin, M. Maglione, V.A. Antohe, G. Hamoir, F. Abreu Araujo, L. Piraux, Synthesis and magnetic properties of Ni–

- BaTiO₃ nanocable arrays within ordered anodic alumina templates. *J. Mater. Chem. C* **3**, 107–111 (2015)
12. A.O. Turkey, M.M. Rashad, M. Bechelany, Tailoring optical and dielectric properties of Ba_{0.5}Sr_{0.5}TiO₃ powders synthesized using citrate precursor route. *Mater. Des.* **90**, 54–59 (2016)
 13. A.O. Turkey, M.M. Rashad, A.T. Kandil, M. Bechelany, Tuning the optical, electrical and magnetic properties of Ba_{0.5}Sr_{0.5}Ti_{1-x}M_{1-x}O₃ (BST) nanopowders. *Phys. Chem. Chem. Phys.* **17**, 12553–12560 (2015)
 14. R. Sharma, P. Pahuja, R.P. Tandon, Structural, dielectric, ferromagnetic, ferroelectric and ac conductivity studies of the BaTiO₃-CoFe_{1.8}Zn_{0.2}O₄ multiferroic particulate composites. *Ceram. Int.* **40**, 9027–9036 (2014)
 15. R.M. Mohamed, M.M. Rashad, F.A. Haraz, W. Sigmund, Magnetic nanocomposite based on titania-silica/cobalt ferrite for photocatalytic degradation of methylene blue dye. *J. Magn. Magn. Mater.* **322**, 2058–2064 (2014)
 16. M.A. Ahmed, S.F. Mansour, M. Afifi, Structural, electric and magnetoelectric properties of Ni_{0.85}Cu_{0.15}Fe₂O₄/BiFe_{0.7}Mn_{0.3}O₃ multiferroic nanocomposites. *J. Alloys Compd.* **578**, 303–308 (2013)
 17. D. Vaishnav, R.K. Goyal, Thermal and dielectric properties of high performance polymer/ZnO nanocomposites. *Mater. Sci. Eng.* **64**, 012016 (2014)
 18. M.M. Rashad, M. Rasly, H.M. El-Sayed, A.A. Sattar, I.A. Ibrahim, Controlling the composition and the magnetic properties of hexagonal Co₂Z ferrite powders synthesized using two different methods. *Appl. Phys. A* **112**(4), 963–973 (2013)
 19. A. Goldman, *Modern Ferrite Technology*, 2nd edn. (Springer, Pittsburgh, 2006)
 20. M. Rasly, M.M. Rashad, Structural and magnetic properties of Sn-Zn doped BaCo₂Z-type hexaferrite powders prepared by citrate precursor method. *J. Magn. Magn. Mater.* **337**, 58–64 (2013)
 21. L.M. Salah, M.M. Rashad, M. Haroun, M. Rasly, M.A. Soliman, Magnetically roll-oriented LaFeO₃ nanospheres prepared using oxalic acid precursor method. *J. Mater. Sci. Mater. Electron.* **26**, 1045–1052 (2015)
 22. E.V. Ramana, F. Figueiras, M.P.F. Graça, M.A. Valente, Observation of magnetoelectric coupling and local piezoresponse in modified (Na_{0.5}Bi_{0.5})TiO₃-BaTiO₃-CoFe₂O₄ lead-free composites. *Dalton Trans.* **43**, 9934–9943 (2014)
 23. S.N. Babu, K. Srinivas, T. Bhima, Sankaram, Studies on lead-free multiferroic magnetoelectric composites. *J. Magn. Magn. Mater.* **321**(22), 3764–3770 (2009)
 24. S.C. Yang, C.W. Ahn, K.H. Cho, S. Priya, Self-bias response of lead-free (1-x)[0.948 K_{0.5}Na_{0.5}NbO₃-0.052 LiSbO₃]-xNi_{0.8}Zn_{0.2}Fe₂O₄-Nickel magnetoelectric laminate composites. *J. Am. Ceram. Soc.* **94**(11), 3889–3899 (2011)
 25. O.G. Udalov, N.M. Chitchev, I.S. Beloborodov, Coupling of ferroelectricity and ferromagnetism through Coulomb blockade in composite multiferroics. *Phys. Rev. B* **89**, 174203 (2014)